Int. J. Heat Mass Transfer. Vol. 29, No. 5, pp. 659–671, 1986
Printed in Great Britain

0017–9310/86 $3.00 + 0.00
Pergamon Journals Ltd.

Heat transfer inside a horizontal cylindrical annulus in the presence of thermal radiation and buoyancy

S. O. ONYEGEGBU
Department of Mechanical Engineering, University of Nigeria, Nsukka, Nigeria

(*Received* 20 *February* 1984 *and in final form* 3 *September* 1985)

Abstract—Heat transfer in an absorbing and emitting nongray Boussinesq fluid within the annular gap of two infinitely long isothermal horizontal concentric cylinders is studied analytically. The Milne–Eddington approximation is employed in expressing the two-dimensional radiative transfer to include radial and tangential radiation. Results indicate that decreasing Planck number, increasing the degree of nongrayness of the fluid or increasing optical thickness increases the total heat transfer and reduces the induced buoyant flow intensity and velocities. Decreasing boundary emissivity produces the opposite effect. Because radiation decreases a fluid's effective Prandtl number, increasing radiation causes a downward movement of the centre of the eddy formed with medium Prandtl number fluids like air.

INTRODUCTION

THE PROBLEM of heat transfer inside the annulus between two horizontal cylinders in the presence of convection and radiation represents an idealization of many meaningful problems in engineering practice. Some of these problems include solar heat collection using concentrators, heat removal from gas-cooled fast reactors, design of high-temperature heat exchangers and heat removal from many electrical and electronic equipments, amongst many others. Because of the complexities involved in formulating and solving these problems, it is common to neglect radiative effects and consider only the relatively low-temperature-level problems, hence solving only the natural convection problem in cylindrical annuli. Experimental and analytical simulations of these buoyancy-driven flows have received a great deal of attention in the literature [1–7]. These papers have studied the nature of the induced convection currents which control the heat transfer process. Results show that for both high- and low-Prandtl-number fluids in an annulus there is a critical Rayleigh number below which the convective flow patterns are steady and laminar and above which the flow patterns are unsteady and, in fact, oscillatory. Powe *et al.* [3] also reported that for inverse relative gap widths greater than about 2.8, stable secondary cellular flows consisting of steady counter-rotating eddy pairs occurred in the upper region of the annulus for Rayleigh numbers slightly below critical. From a heat transfer point of view, the Nusselt number behaviour is of primary importance. The results of Powe *et al.* [4] indicate a variation in the average Nusselt number independent of the type of flow, however, the local Nusselt number was found to be higher at locations where secondary flow exists.

As has been indicated, the above-mentioned results are for the low-temperature-level applications where radiative effects are not significant or have been neglected. Because of the high temperature levels required in many modern technology systems, the need arises to extend the problem discussed above to include the radiative effects of the participating fluid as well as of the boundaries. This requires writing the radiative transfer equation for cylindrical geometry. The literature on radiative transfer in non-Cartesian geometry is fairly scanty. Some authors [8–11] have expressed the cylindrical radiative transfer equation in the form of an integro-differential equation which is tedious to solve. Perlmutter and Howell [12] solved the problem of radiant heat transfer through a gray gas between concentric cylinders using the Monte-Carlo method. This formulation, though accurate, is computationally expensive because a large number of probable paths of discrete energy bundles must be constructed and followed in order to obtain statistically meaningful results. A simple model based on the Milne–Eddington approximation, which can be derived by the method of moments or spherical harmonics has been used [13–15] to describe thermal radiation in cylindrical geometry. This permits the formulation of the radiative transfer equation in terms of a differential equation. These formulations have been proposed for axially symmetric problems or one-dimensional problems where tangential radiation is assumed negligible when compared with radial radiation. In problems where temperature is expected to vary in the tangential direction, due to buoyancy, it may not be convenient to *a priori* assume tangential radiation to be small. However, the Milne–Eddington differential approximation is easily amenable to a formulation including tangential radiation. Additional advantages of this approximation are that the weighted nongrayness of the participating fluid as well as the radiative colour of the boundaries are incorporated in the formulation. Arpaci and Gozum [16] studied the accuracy of this approximation by comparing its results with those of the exact solution for a Cartesian

NOMENCLATURE

B Planck function
C_p specific heat at constant pressure
g acceleration due to gravity
I frequency-averaged radiative intensity
J dimensionless first moment of radiative intensity
K thermal conductivity
Nu local Nusselt number
$\overline{Nu}$ average Nusselt number
P pressure
Pl Planck number, $\alpha_m K/4\sigma T_i^{*3}$
Pr Prandtl number, ν/κ
q_r^R radial radiative heat flux
q_θ^R tangential radiative heat flux
r dimensionless radial position
R radius ratio, r_o^*/r_i^*
Ra Rayleigh number, $g\beta(T_i^* - T_o^*)r_i^{*3}/k\nu$
T dimensionless temperature
T' Temperature ratio of outer boundary to inner boundary, T_o^*/T_i^*
U dimensionless radial velocity
V dimensionless tangential velocity.

Greek symbols

α_C Chandrasekhar mean absorption coefficient
α_E Einstein mean absorption coefficient
α_m mean absorption coefficient, $(\alpha_P\alpha_R)^{1/2}$
α_P Planck mean absorption coefficient
α_R Rosseland mean absorption coefficient
β coefficient of thermal expansion
γ the azimuth angle of radiation ray
ε hemispherical (diffuse) emissivity of the boundary
η degree of nongrayness of fluid $(\alpha_P/\alpha_R)^{1/2}$
θ angular position measured counter-clockwise from the downward vertical
κ thermal diffusivity
μ dynamic viscosity
ν kinematic viscosity
ρ fluid density
σ Stefan–Boltzman constant
τ optical thickness, $\alpha_m r_i^*$
ϕ angle between a radiation ray and the radial direction
ψ dimensionless streamfunction.

Subscripts

i inner boundary
o outer boundary
ci convective quantity on the inner boundary
co convective quantity on the outer boundary
ri radiative quantity on the inner boundary
ro radiative quantity on the outer boundary
λ monochromatic quantity.

Superscripts

* dimensional quantity.

geometrical problem. They found that the approximation gave adequate results for intermediate optical thickness in addition to the known fact that it gives the exact results for the thin gas case, $\tau \to 0$, and for the thick gas case, $\tau \to \infty$.

This paper deals with the problem of heat transfer inside horizontal concentric cylinders in the presence of radiation, buoyancy and conduction. The problem, including the radiative transfer equation, is formulated in a two-dimensional cylindrical co-ordinate, the radial and tangential directions. The effect of radiation on the well-established streamline pattern, particularly on the development of secondary cellular flows, if any, is studied.

FORMULATION

Consider an absorbing and emitting nongray Boussinesq fluid in the annular gap between two infinitely long horizontal concentric cylinders. The walls are isothermal with the inside wall maintained at a temperature T_i^* and the outside wall maintained at a lower temperature T_o^*. A cylindrical polar co-ordinates system is taken with the angular position θ measured counter-clockwise from the downward vertical through the centre and the radial distance r^* measured from the centre. The problem is symmetric about the vertical diameter and so attention is confined to the region bounded by $0 \leqslant \theta \leqslant \Pi$. Neglecting the contribution of radiative stress to the momentum equations, we can express the continuity, radial momentum, tangential momentum and energy equations as

$$\frac{1}{r^*}\frac{\partial}{\partial r^*}(r^*U^*) + \frac{1}{r^*}\frac{\partial V^*}{\partial \theta} = 0 \tag{1}$$

$$\rho\left\{U^*\frac{\partial U^*}{\partial r^*} + \frac{V^*}{r^*}\frac{\partial U^*}{\partial \theta} - \frac{V^{*2}}{r^*}\right\} = -\frac{\partial P}{\partial r^*} + \mu\left[\frac{\partial}{\partial r^*}\left\{\frac{1}{r^*}\frac{\partial}{\partial r^*}(r^*U^*)\right\} + \frac{1}{r^{*2}}\frac{\partial^2 U^*}{\partial \theta^2} - \frac{2}{r^{*2}}\frac{\partial V^*}{\partial \theta}\right] + \rho g\{1 - \beta(T^* - T_o^*)\}\cos\theta \tag{2}$$

$$\rho\left\{U^*\frac{V^*}{r^*} + \frac{V^*}{r^*}\frac{\partial V^*}{\partial \theta} + \frac{U^*V^*}{r^*}\right\} = -\frac{1}{r^*}\frac{\partial P}{\partial \theta} + \mu\left[\frac{\partial}{\partial r^*}\left\{\frac{1}{r^*}\frac{\partial}{\partial r^*}(r^*V^*)\right\} + \frac{1}{r^{*2}}\frac{\partial^2 V^*}{\partial \theta^2} + \frac{2}{r^{*2}}\frac{\partial U^*}{\partial \theta}\right] - \rho g\{1 - \beta(T^* - T_o^*)\}\sin\theta \tag{3}$$

$$\rho C_p\left\{U^*\frac{\partial T^*}{\partial r^*}+\frac{V^*}{r}\frac{\partial T^*}{\partial\theta}\right\}=K\left\{\frac{1}{r^*}\frac{\partial}{\partial r^*}\left(r^*\frac{\partial T^*}{\partial r^*}\right)+\frac{1}{r^{*2}}\frac{\partial^2 T^*}{\partial\theta^2}\right\}-\frac{1}{r^*}\frac{\partial}{\partial r^*}(r^* q_r^R)-\frac{1}{r^*}\frac{\partial q_\theta^R}{\partial\theta}. \quad (4)$$

The energy equation (4) contains the radiative heat fluxes in the radial and tangential directions, and these will be evaluated using the method of moments coupled with the assumption of local isotropy for radiative intensity, which is the Milne–Eddington approximation. The resulting equations are identical to those obtained as the $P-1$ approximation when radiative intensity is expanded in a series of spherical harmonics. The two-dimensional monochromatic photon balance (radiative transfer equation) written in cylindrical r^* and θ co-ordinates is

$$\cos\phi\frac{\partial I_\lambda}{\partial r^*}+\frac{\sin\phi\cos\gamma}{r^*}\frac{\partial I_\lambda}{\partial\theta}=\alpha_\lambda(B_\lambda-I_\lambda) \quad (5)$$

where $\cos\phi$ is the radial component of the unit vector in a ray direction, and $\sin\phi\cos\gamma$ is the tangential component of the same vector. The first moment of the transfer equations is obtained by integrating equation (5) over all solid angles and frequencies and, if the blackbody radiation is related to temperature, one obtains

$$\frac{\partial q_r^R}{\partial r^*}+\frac{1}{r^*}\frac{\partial q_\theta^R}{\partial\theta}=4\alpha_P\sigma T^{*4}-\alpha_E J^* \quad (6)$$

where

$$q_r^R=\int_0^\infty\int_0^{2\pi}\int_0^\pi I_\lambda\sin\phi\cos\phi\,d\phi\,d\gamma\,d\lambda \quad (7)$$

$$q_\theta^R=\int_0^\infty\int_0^{2\pi}\int_0^\pi I_\lambda\sin^2\phi\cos\gamma\,d\phi\,d\gamma\,d\lambda \quad (8)$$

$$\alpha_P=\frac{\int_0^\infty\alpha_\lambda B_\lambda\,d\lambda}{\int_0^\infty B_\lambda\,d\lambda} \quad (9)$$

$$\alpha_E=\frac{\int_0^\infty\alpha_\lambda I_\lambda\,d\lambda}{\int_0^\infty I_\lambda\,d\lambda} \quad (10)$$

and

$$J^*=\int_0^\infty\int_0^{2\pi}\int_0^\pi I_\lambda\sin\phi\,d\phi\,d\gamma\,d\lambda. \quad (11)$$

The second radial moment of the transfer equation is obtained by multiplying equation (5) by $\cos\phi$ and integrating over all solid angles and frequencies to get

$$\frac{\partial H}{\partial r^*}+\frac{1}{r^*}\frac{\partial L}{\partial\theta}=-\alpha_R q_r^R \quad (12)$$

$$H=\int_0^\infty\int_0^{2\pi}\int_0^\pi I_\lambda\cos^2\phi\sin\phi\,d\phi\,d\gamma\,d\lambda \quad (13)$$

$$L=\int_0^\infty\int_0^{2\pi}\int_0^\pi I_\lambda\sin^2\phi\cos\phi\cos\gamma\,d\phi\,d\gamma\,d\lambda \quad (14)$$

$$\alpha_C=\frac{\int_0^\infty\alpha_\lambda q_{r\lambda}^R\,d\lambda}{\int_0^\infty q_{r\lambda}^R\,d\lambda} \quad (15)$$

and

$$q_{r\lambda}^R=\int_0^{2\pi}\int_0^\pi I_\lambda\sin\phi\cos\phi\,d\phi\,d\lambda. \quad (16)$$

Using the assumption of local isotropy, which is that I_λ is neither a function of ϕ nor of γ, equations (11), (13) and (14) are integrated to get

$$J^*=4\pi I \quad (17)$$

$$H=\frac{4\pi}{3}I \quad (18)$$

$$L=0 \quad (19)$$

where

$$I=\int_0^\infty I_\lambda\,d\lambda.$$

With local isotropy also, $\alpha_E=\alpha_P$ and $\alpha_C=\alpha_R$ where

$$\frac{1}{\alpha_R}=\frac{\int_0^\infty\frac{1}{\alpha_\lambda}\frac{\partial B_\lambda}{\partial T^*}\,d\lambda}{\int_0^\infty\frac{\partial B_\lambda}{\partial T^*}\,d\lambda}.$$

Equations (17) and (18) are now combined to give $H=J^*/3$ which is substituted into equation (12) to get

$$\frac{1}{3}\frac{\partial J^*}{\partial r^*}=-\alpha_R q_r^R. \quad (20)$$

The second tangential moment of the transfer equation is obtained by multiplying equation (5) by $\sin\phi\cos\gamma$ and integrating over all solid angles and frequencies to get

$$\frac{1}{r^*}\frac{\partial G}{\partial\theta}=-\alpha_R q_\theta^R \quad (21)$$

where

$$G=\int_0^\infty\int_0^{2\pi}\int_0^\pi I_\lambda\sin^3\phi\cos^2\gamma\,d\phi\,d\gamma\,d\lambda$$

and for local isotropy,

$$G=\frac{4\pi}{3}I=\frac{J^*}{3}$$

which when substituted into equation (21) gives

$$\frac{1}{3r^*}\frac{\partial J^*}{\partial\theta}=-\alpha_R q_\theta^R. \quad (22)$$

Equations (20) and (21) are then substituted into the

energy equation (4) to get

$$\rho C_p \left\{ U^* \frac{\partial T^*}{\partial r^*} + \frac{V^*}{r^*} \frac{\partial T^*}{\partial \theta} \right\} = K \left\{ \frac{1}{r^*} \frac{\partial}{\partial r^*} \left(r^* \frac{\partial T}{\partial r^*} \right) + \frac{1}{r^{*2}} \frac{\partial^2 T^*}{\partial \theta^2} \right\} + \frac{1}{3} \alpha_R \left\{ \frac{\partial^2 J^*}{\partial r^{*2}} + \frac{1}{r^*} \frac{\partial J^*}{\partial r^*} + \frac{1}{r^{*2}} \frac{\partial^2 J^*}{\partial \theta^2} \right\}. \quad (23)$$

Using equations (20) and (22) in equation (6), the integrated radiative transfer equation becomes

$$\frac{\partial^2 J^*}{\partial r^{*2}} + \frac{1}{r^*} \frac{\partial J^*}{\partial r^*} + \frac{1}{r^{*2}} \frac{\partial^2 J^*}{\partial \theta^2} - 3\alpha_p \alpha_R J^* = -12 \alpha_p \alpha_R \sigma T^{*4}. \quad (24)$$

Equations (1)–(3), (23) and (24) constitute the governing equations for the problem. If a streamfunction consistent with equation (1) is defined by

$$U^* = \frac{1}{r^*} \frac{\partial \psi^*}{\partial \theta} \quad \text{and} \quad V^* = -\frac{\partial \psi^*}{\partial r^*} \quad (25)$$

equations (2) and (3) can be combined by cross differentiation to eliminate the pressure terms and the resulting governing equations in dimensionless form become

$$\nabla^4 \psi = Ra \left(\sin\theta \frac{\partial T}{\partial r} + \frac{\cos\theta}{r} \frac{\partial T}{\partial \theta} \right) + \frac{1}{rPr} \frac{\partial (\nabla^2 \psi, \psi)}{\partial (r, \theta)} \quad (26)$$

$$\nabla^2 T = \frac{1}{r} \frac{\partial (T, \psi)}{\partial (r, \theta)} - \frac{\eta}{Pl} \nabla^2 J \quad (27)$$

$$\nabla^2 J - 3\tau^2 J = -\tau^2 \left(\frac{1}{1 - T'} \right) \{ T' + (1 - T') T \}^4 \quad (28)$$

where the following dimensionless variables have been introduced

$$r = \frac{r^*}{r_i^*}, \quad \psi = \frac{\psi^*}{\kappa}, \quad T = \frac{T^* - T_o^*}{T_i^* - T_o^*}, \quad J = \frac{J^*}{12 \sigma T_i^{*3} (T_i^* - T_o^*)}.$$

The dimensionless velocities now become

$$U = \frac{1}{r} \frac{\partial \psi}{\partial \theta} \quad \text{and} \quad V = -\frac{\partial \psi}{\partial r}. \quad (29)$$

The Jacobian and Del operators are defined symbolically as

$$\frac{\partial (f, g)}{\partial (r, \theta)} = \frac{\partial f}{\partial r} \frac{\partial g}{\partial \theta} - \frac{\partial f}{\partial \theta} \frac{\partial g}{\partial r}$$

$$\nabla^2 = \frac{\partial}{\partial r^2} + \frac{1}{r} \frac{\partial}{\partial r} + \frac{1}{r^2} \frac{\partial^2}{\partial \theta^2}$$

$$\nabla^4 = \nabla^2 (\nabla^2).$$

The dimensionless boundary conditions are readily determined as follows:

$$\psi = \frac{\partial \psi}{\partial r} = 0 \quad \text{at} \quad r = 1, R$$

$$T = 1 \quad \text{at} \quad r = 1 \quad \text{and} \quad T = 0 \quad \text{at} \quad r = R$$

for symmetry about $\theta = 0, \pi$,

$$\psi = \frac{\partial^2 \psi}{\partial \theta^2} = \frac{\partial T}{\partial \theta} = 0 \quad \text{at} \quad \theta = 0, \pi.$$

The corresponding radiative boundary conditions are developed along similar lines as ref. [16] and these are

$$J = (\eta / 3\chi\tau) \frac{\partial J}{\partial r} + \frac{1}{3(1 - T')} \quad \text{at} \quad r = 1$$

$$J = (\eta / 3\chi\tau) \frac{\partial J}{\partial r} + \frac{T'^4}{3(1 - T')} \quad \text{at} \quad r = R$$

$$\frac{\partial J}{\partial \theta} = 0 \quad \text{at} \quad \theta = 0, \pi$$

where

$$\chi = \frac{\varepsilon}{2(2 - \varepsilon)}.$$

METHOD OF SOLUTION

A number of methods have been proposed for solving the governing partial differential equations that result when considering convection in enclosed fluids. Orzag and Israeli [17] recommend the method of spectral expansion using trigonometric functions when the enclosure is cylindrical and symmetrical. This method was tried first, however, for a three-term trigonometric series, the solution of the resulting ordinary differential equations using matrix inversion required much computer storage and time, and convergence could not be guaranteed even for medium value Rayleigh numbers. Solution by perturbation techniques also limits the range of applicability of any results obtained. The direct finite-difference scheme was therefore resorted to. One typical method of this scheme is to first solve for the vorticity funcion, calculate the streamfunction from the vorticity and then proceed to solve temperature and radiative intensity equations. This method was not adopted because of the inaccuracies involved in expressing the vorticity boundary conditions.

A numerical solution was obtained by approximating the derivatives of equations (26)–(28) by their central difference equivalents, thereby transforming the equations into coupled difference equations. The simple Gauss–Siedel iterative method was then used to obtain solutions for each equation. The nonlinearity of the governing equations necessitates the use of another iterative cycle before solutions can be obtained. The order is to solve first for temperature, then for radiative intensity and then for the streamfunction. This $T-J-\psi$ cycle was continued until the sums of the absolute

values of the deviations of $T_{i,j}$, $J_{i,j}$ and $\psi_{i,j}$ from their previous values were each less than 10^{-3}. Once satisfactory T, J and ψ have been found, the dimensionless radial and tangential velocities can then be computed. Several other methods have been proposed by de Vahl Davis [18] and Prakash and Patankar [19] to ensure the stability and convergence of the coupled difference equations at increased Rayleigh numbers, but the simplicity of the Gauss–Siedel method was preferred to this slight increase in the range of applicability.

For heat transfer calculations, local Nusselt numbers made up of convective and radiative components were defined at any annular position for the inner and outer boundaries of the annulus. For the inner boundary, the expression is

$$Nu_i = -\frac{\partial T}{\partial r} - \frac{\eta}{Pl}\frac{\partial J}{\partial r} \quad \text{at} \quad r = 1 \tag{30}$$

and for the outer boundary,

$$Nu_o = -R\frac{\partial T}{\partial r} - \frac{\eta}{Pl}\frac{\partial J}{\partial r} \quad \text{at} \quad r = R. \tag{31}$$

The first term on the RHS of each expression represents convective Nusselt number while the second term is the radiative Nusselt number. The average Nusselt number at each boundary is obtained by numerically integrating each expression over the angular domain of 0° to 180°.

Convergence and accuracy tests were carried out by increasing the number of grid points, increasing the number of iterations in the Gauss–Siedel solutions, increasing the number of iterations in the $T-J-\psi$ cycle and evaluating the discrepancy between the average Nusselt number of both boundaries. An increased number of grid points and iterations were necessary for convergence with higher values of Ra, η, τ and lower values of Pl. The streamfunction equation was found to converge in all cases examined when $Ra(\Delta r)^3 < 1.0$ while the temperature equation converged when $\eta\tau^2\Delta r/Pl < 1.0$. Thirty-six grid spacings in the angular direction and 20 in the radial direction were found to be adequate for results presented; 250 iterations in the Gauss–Siedel loop were used for the temperature equation, 400 iterations for the radiative intensity equation and as much as 800 iterations were required for the streamfunction equation. The adequate number of $T-J-\psi$ iteration cycles varied from 4 to 8 with the higher Ra and lower Pl cases requiring more cycles. The discrepancy in the values of the average Nusselt numbers on both boundaries arises mainly from truncation errors encountered in the finite-difference scheme [20], and so could be used as a measure of the accuracy of the finite-difference method. A fairly good agreement is observed except at high radiation level cases of $Pl = 0.01$ where as much as 30 grid spacings in the radial direction did not resolve the discrepancy.

NUMERICAL RESULTS AND CONCLUSIONS

Numerical results presented are for a gaseous fluid medium, which is more susceptible to radiation effects, and the Prandtl number is taken as 0.7. To lessen the number of numerical calculations, only one temperature ratio, $T' = 0.2$ was considered. The values of radiation parameters employed are in the range known to be reasonable for gases [16]. Thermal radiation effects on heat transfer, temperature, velocities and streamfunctions were evaluated for Rayleigh numbers slightly below and slightly above the transition values given by Powe *et al.* [4].

The heat transfer information is summarized in Table 1 and gives the calculated average convective, radiative and total Nusselt number on both the inner and outer boundaries of the annulus as well as the extreme values of velocities and streamfunctions attained for stated conditions. The results show that radiation does significantly affect heat transfer inside a cylindrical annulus. For a fixed Rayleigh number and radius ratio, increasing τ or η as well as decreasing Pl (increasing radiation parameters) results in a decrease of the average convective Nusselt number and an increase of the average radiative Nusselt number on the inner boundary of the annulus. The increase in the radiative Nusselt number predominates over the slight decrease in convective Nusselt number giving rise to an increase of the average total Nusselt number. On the outer boundary, because of the lower temperature level, radiative increases of the average radiative Nusselt number is less than on the inside. Unlike the inside, radiation increases the average convective Nusselt number in order to keep the average total Nusselt number the same on both boundaries. Hence with an emitting, absorbing fluid at a high temperature, radiative transfer is the dominant heat transfer mechanism on the inner boundary of the annulus while convection becomes an important heat transfer mechanism on the outer boundary. The other radiation parameter, surface emissivity, on being decreased, increases the average convective Nusselt number on the inside while decreasing it on the outside. For the limiting case when surface emissivity is zero, that is the case of mirror boundaries, there is no radiative transfer at the boundaries and so the average total Nusselt number is less than that for the case of black boundaries, even on the inside where reduced surface emissivity increases the convective Nusselt number. From the tabulated values of the average total Nusselt numbers, it is evident that for maximum heat extraction from a hot inner cylinder to a cold outer cylinder, one would need to employ a highly emitting and absorbing fluid coupled with high emissivity boundaries. It is interesting to note that the average radiative Nusselt number is almost independent of Rayleigh number and radius ratio. Figures 1 and 2 respectively show radiative effects on local radiative and convective Nusselt numbers around the annulus boundaries. On the inside, convective and radiative transfers are

Table 1. Summary of the dependence of the average heat transfer and induced flow on radiation parameters

R	Ra	Pl	τ	η	ε	$\overline{Nu}_{ci}$	$\overline{Nu}_{ri}$	Nu_i	$\overline{Nu}_{co}$	$\overline{Nu}_{ro}$	$\overline{Nu}_o$	Extreme tangential velocity and its location	Extreme radial velocity and its location	Extreme stream function and its location
1.5	10^4	1.0	1.0	1.0	1.0	2.5016	0.3097	2.8113	2.6117	0.2028	2.8145	$V = 17.5766$ $r = 1.1$ $\theta = 90°$	$U = 2.4497$ $r = 1.25$ $\theta = 170°$	$\psi = -2.7726$ $r = 1.25$ $\theta = 90°$
1.5	10^4	0.1	1.0	1.0	1.0	2.4212	3.0478	5.4690	3.3850	1.3907	4.7757	$V = 16.8123$ $r = 1.1$ $\theta = 90°$	$U = 2.3339$ $r = 1.25$ $\theta = 170°$	$\psi = -2.7046$ $r = 1.25$ $\theta = 90°$
1.5	10^4	1.0	5.0	1.0	1.0	2.3957	0.8367	3.2324	3.0912	0.0948	3.1860	$V = 17.2252$ $r = 1.1$ $\theta = 90°$	$U = 2.3834$ $r = 1.25$ $\theta = 170°$	$\psi = -2.7685$ $r = 1.25$ $\theta = 90°$
1.5	10^4	1.0	0.0	1.0	1.0	2.5203	—	2.5203	2.5212	—	2.5212	$V = 17.6562$ $r = 1.1$ $\theta = 90°$	$U = 2.4624$ $r = 1.25$ $\theta = 170°$	$\psi = -2.7783$ $r = 1.25$ $\theta = 90°$
1.5	10^4	1.0	1.0	1.0	0.0	2.5646	—	2.5646	2.5652	—	2.5652	$V = 17.5608$ $r = 1.1$ $\theta = 90°$	$U = 2.4467$ $r = 1.25$ $\theta = 170°$	$\psi = -2.7655$ $r = 1.25$ $\theta = 90°$
1.2	10^4	1.0	1.0	1.0	1.0	5.4639	0.3239	5.7878	5.5408	0.2157	5.7565	$V = 2.8490$ $r = 1.04$ $\theta = 90°$	$U = 0.1678$ $r = 1.10$ $\theta = 170°$	$\psi = -0.1838$ $r = 1.10$ $\theta = 90°$
1.2	10^4	0.01	1.0	1.0	1.0	5.0309	31.3685	36.3994	9.5961	22.5386	32.1347	$V = 2.4505$ $r = 1.04$ $\theta = 90°$	$U = 0.1502$ $r = 1.10$ $\theta = 170°$	$\psi = -0.1648$ $r = 1.10$ $\theta = 90°$
1.2	10^4	1.0	10.0	1.0	1.0	5.2508	1.7540	7.004	6.6113	0.3280	6.9393	$V = 2.7683$ $r = 1.04$ $\theta = 90°$	$U = 0.1656$ $r = 1.10$ $\theta = 170°$	$\psi = -0.1815$ $r = 1.10$ $\theta = 90°$
1.2	10^4	1.0	0.0	1.0	1.0	5.4846	—	5.4846	5.4856	—	5.4846	$V = 2.8524$ $r = 1.04$ $\theta = 90°$	$U = 0.1679$ $r = 1.10$ $\theta = 170°$	$\psi = -0.1839$ $r = 1.10$ $\theta = 90°$
1.2	10^4	0.01	1.0	1.0	0.0	7.3082	—	7.3082	7.0906	—	7.0906	$V = 2.5853$ $r = 1.04$ $\theta = 90°$	$U = 0.1536$ $r = 1.10$ $\theta = 170°$	$\psi = -0.1683$ $r = 1.10$ $\theta = 90°$
1.2	6×10^5	1.0	1.0	1.0	1.0	5.8960	0.3197	6.2157	5.9553	0.2199	6.1752	$V = 178.1593$ $r = 1.04$ $\theta = 85°$	$U = 10.3257$ $r = 1.10$ $\theta = 170°$	$\psi = -11.4079$ $r = 1.10$ $\theta = 90°$

1.2	6×10^5	0.01	1.0	1.0	5.3952	31.3663	36.7615	9.6977	22.5512	32.2489	$V = 167.7479$ $r = 1.16$ $\theta = 90°$	$U = -9.6641$ $r = 1.09$ $\theta = 10°$	$\psi = -10.7086$ $r = 1.10$ $\theta = 85°$
1.2	6×10^5	1.0	10.0	1.0	5.5963	1.7696	7.3659	6.9585	0.3410	7.2995	$V = -173.6994$ $r = 1.16$ $\theta = 95°$	$U = -9.8818$ $r = 1.09$ $\theta = 10°$	$\psi = -11.3369$ $r = 1.10$ $\theta = 90°$
1.2	6×10^5	1.0	0.0	1.0	5.9102	—	5.9102	5.9110	—	5.9110	$V = 178.3313$ $r = 1.04$ $\theta = 85°$	$U = 10.3434$ $r = 1.10$ $\theta = 170°$	$\psi = -11.4130$ $r = 1.10$ $\theta = 90°$
1.2	6×10^5	0.01	1.0	0.0	7.5620	—	7.5620	7.3887	—	7.3887	$V = 162.6141$ $r = 1.04$ $\theta = 85°$	$U = -9.2302$ $r = 1.09$ $\theta = 10°$	$\psi = -10.8251$ $r = 1.10$ $\theta = 90°$
1.2	6×10^5	0.01	1.0	2.0	6.0630	34.3727	40.4257	12.7594	23.2670	36.0264	$V = 152.8892$ $r = 1.16$ $\theta = 90°$	$U = -8.9017$ $r = 1.10$ $\theta = 5°$	$\psi = -9.5254$ $r = 1.10$ $\theta = 85°$

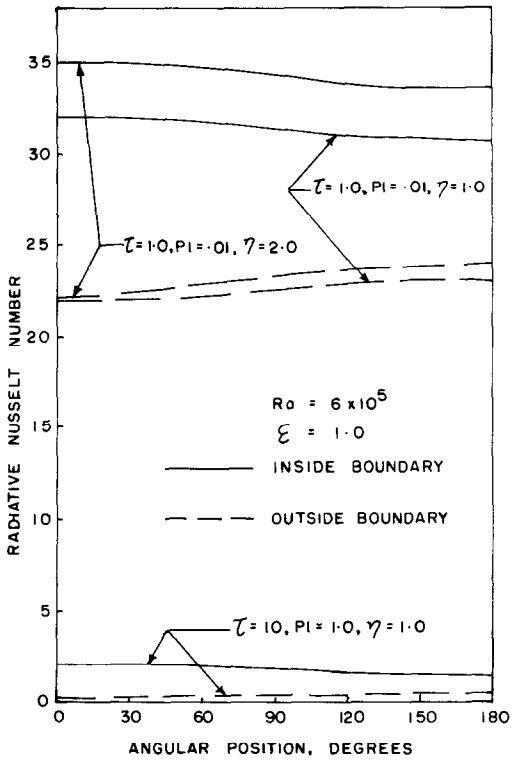

FIG. 1. Radiative effects on radiative heat transfer.

maximum when $\theta = 0°$ while on the outside both are maximum when $\theta = 180°$. The curves for the convective Nusselt number on the inside show that radiation diminishes the angular dependent of local convective Nusselt number while not significantly affecting the local convective Nusselt number on the outside except by uniformly increasing the convective level.

Table 1 also shows the effect of radiation, Rayleigh number and radius ratio on the maximum value of the streamfunctions and velocities in the buoyancy-induced flow. The maximum value of the streamfunction is important in the flow because it is indicative of the flow intensity while also representing the centre of the eddy formation. The table shows that increasing τ, or η or decreasing Pl decreases the intensity of flow while decreased boundary emmissivity increases flow intensity. In most cases the maximum streamfunction occurred at $\theta = 90°$ and midway across the gap except for the high Rayleigh number, high radiation cases. In these cases, when $Pl = 0.01$, $Ra = 6\times10^5$, $R = 1.2$, $\tau = 1.0$, $\varepsilon = 1.0$, and $\eta = 1$ or 2, the maximum stream function occurred at 85°, indicating a downward movement of the centre of the eddy. As noted by ref. [5], this is a characteristic of low-Prandtl-number fluids. It is known from ref. [16] and [21] that radiation reduces the effective Prandtl number of fluids and in the thick gas range the reduction is by a factor of $[1+(4\eta/3Pl)]$. Another consequence of this reduction in effective Prandtl number is manifest in the streamline patterns

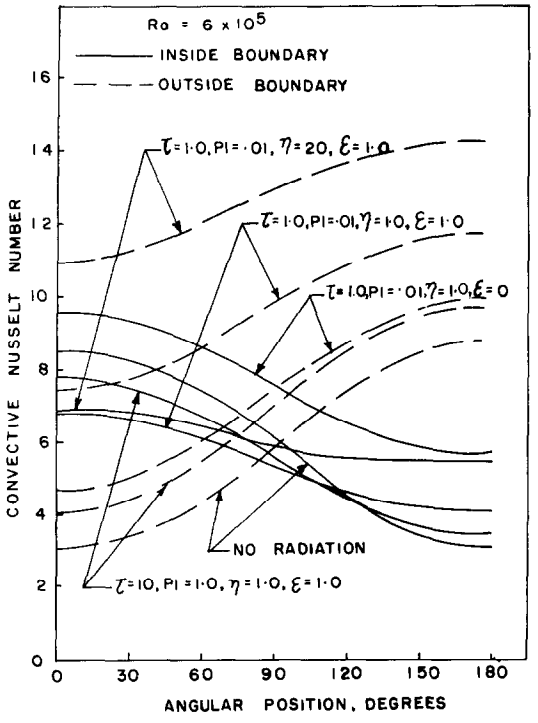

FIG. 2. Radiative effects on convective heat transfer.

(not shown here for brevity) which indicate that the heat transport is dominated by conduction.

The velocity plots are shown in Figs. 3–6 and the trends are consistent with those presented in ref. [4]. The tangential velocity plots exhibit sinusoidal-type behaviour. On the upper half of the annulus, the amplitude of the positive part of the tangential velocity sinusoid is less than the amplitude of the negative part and the reverse is the case on the bottom half. For the case of no radiation and $Ra = 6 \times 10^5$, $R = 1.2$, the crossover point is at $\theta = 100°$. However, for the same Rayleigh number and radius ratio but with $Pl = 0.01$, $\tau = 1.0, \eta = 1$, the crossover point is at $\theta = 65°$ while for $Pl = 1.0$, $\tau = 10.0$, $\eta = 1$, the crossover point is at $\theta = 85°$. Hence radiation does reduce this crossover angle. The radial velocity plots for their part exhibit a maximum or a minimum depending on the angle. The radial velocity is positive and has a maximum on the upper half while it is negative and so has a minimum on the bottom half. The minimum values occurred around $\theta = 10°$ and maximum values occurred around $\theta = 170°$. The higher of the absolute values of the maximum and minimum, as well as location are shown also in Table 1. Powe *et al.* [4] observed secondary flows at the top of the cylinder for a Rayleigh number of 4.5×10^5 and radius ratio of 1.2. In this study, even at a

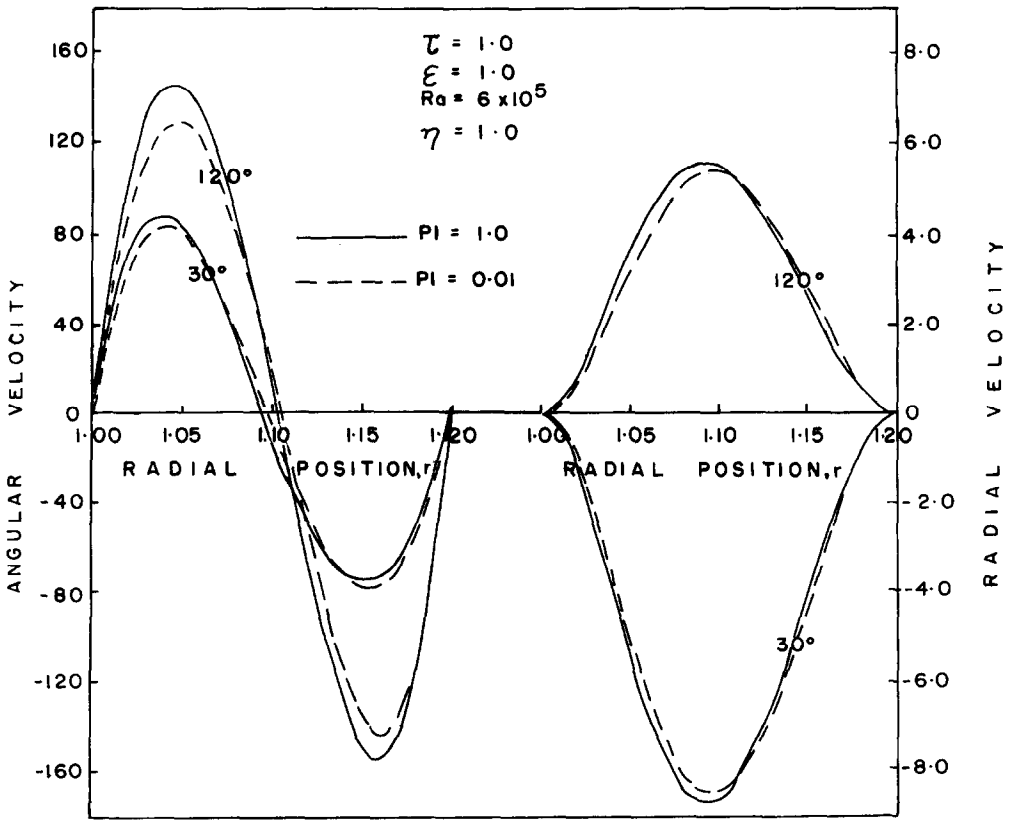

FIG. 3. Effect of Planck number on buoyancy-induced velocities.

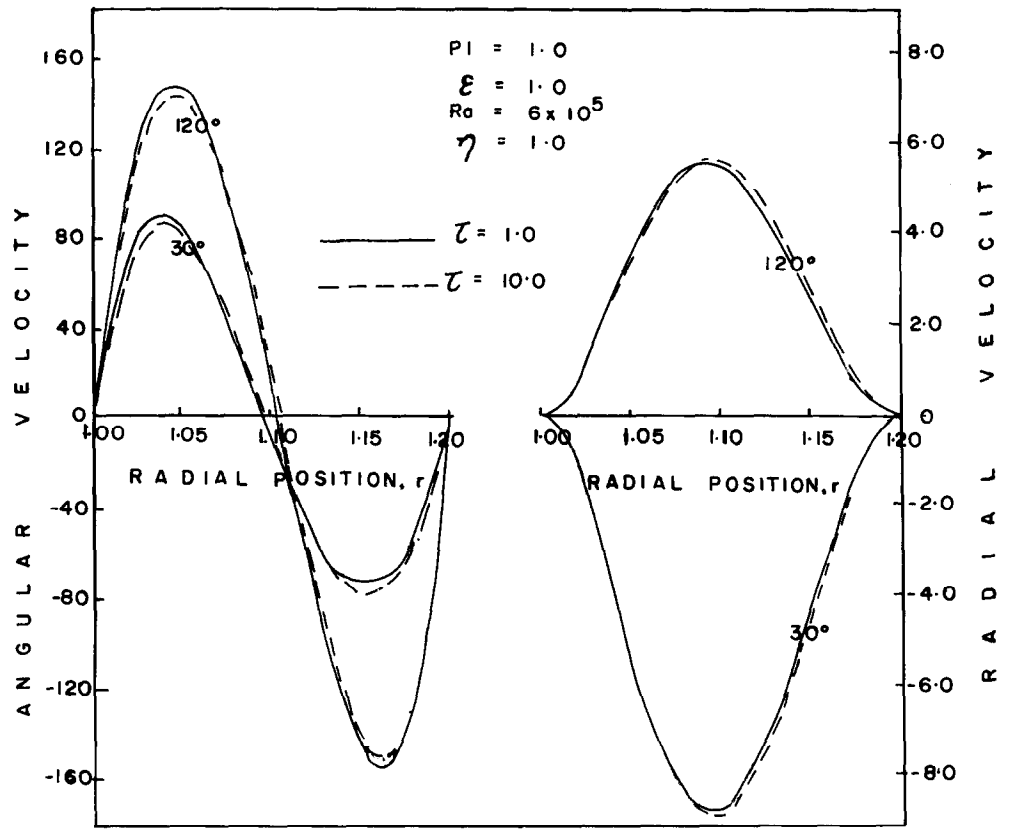

FIG. 4. Effect of optical thickness of fluid on buoyancy-induced velocities.

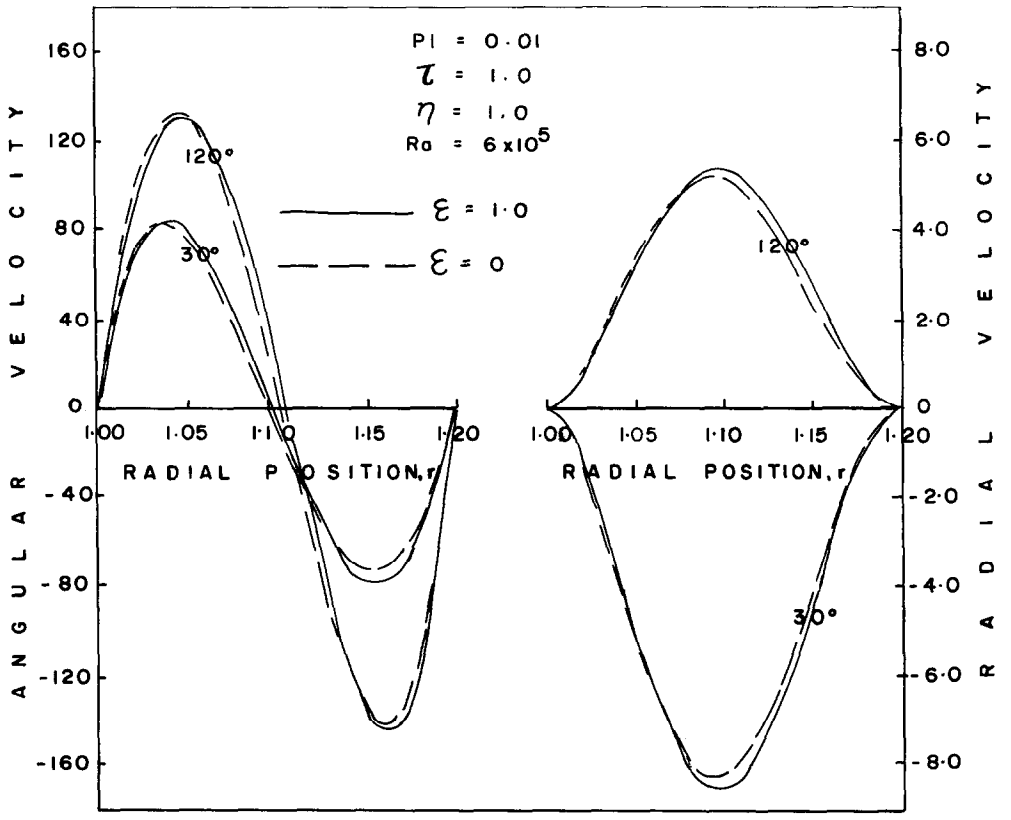

FIG. 5. Effect of boundary surface emissivity on buoyancy-induced velocities.

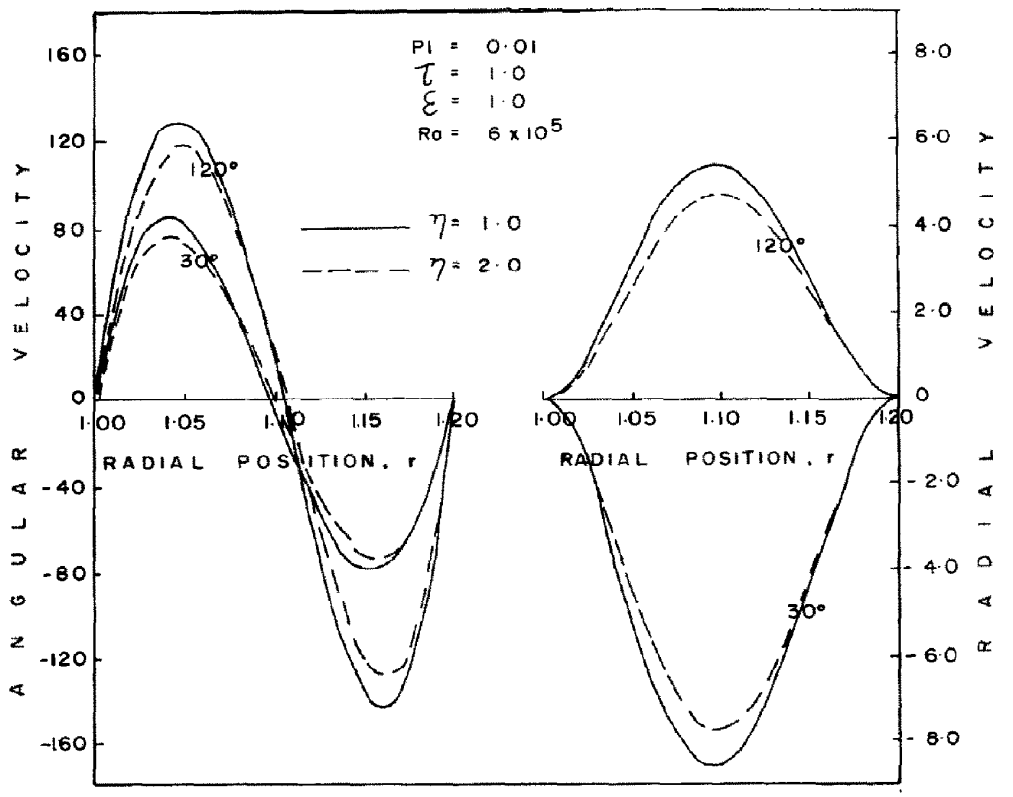

FIG. 6. Effect of the degree of nongrayness of fluid on buoyancy-induced velocities.

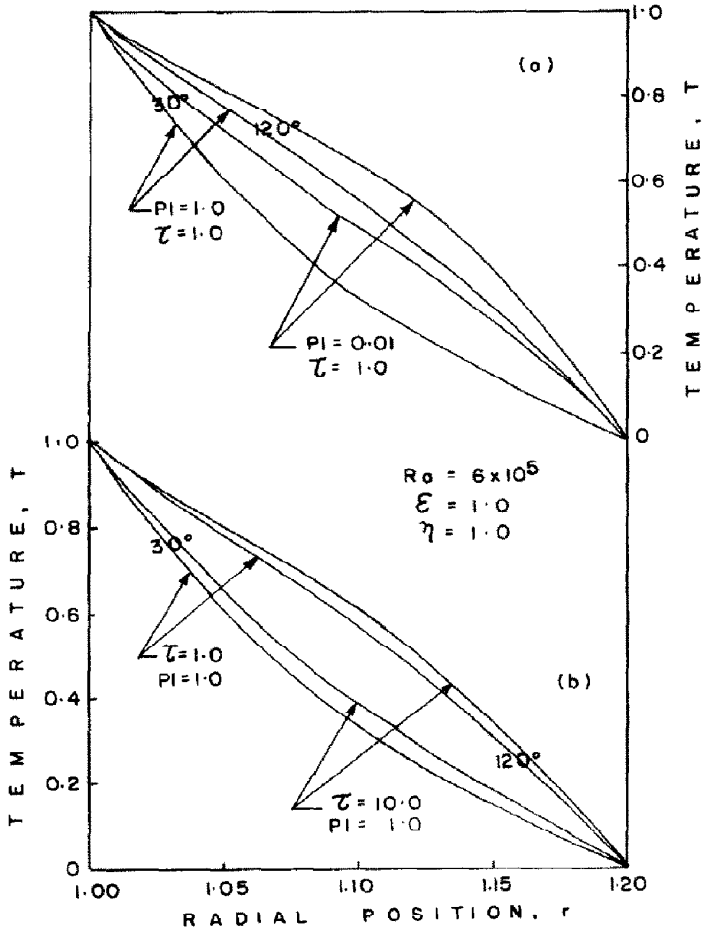

FIG. 7. Temperature profiles for angular positions of 30° and 120°. (a) Effect of Planck number; (b) effect of optical thickness of fluid.

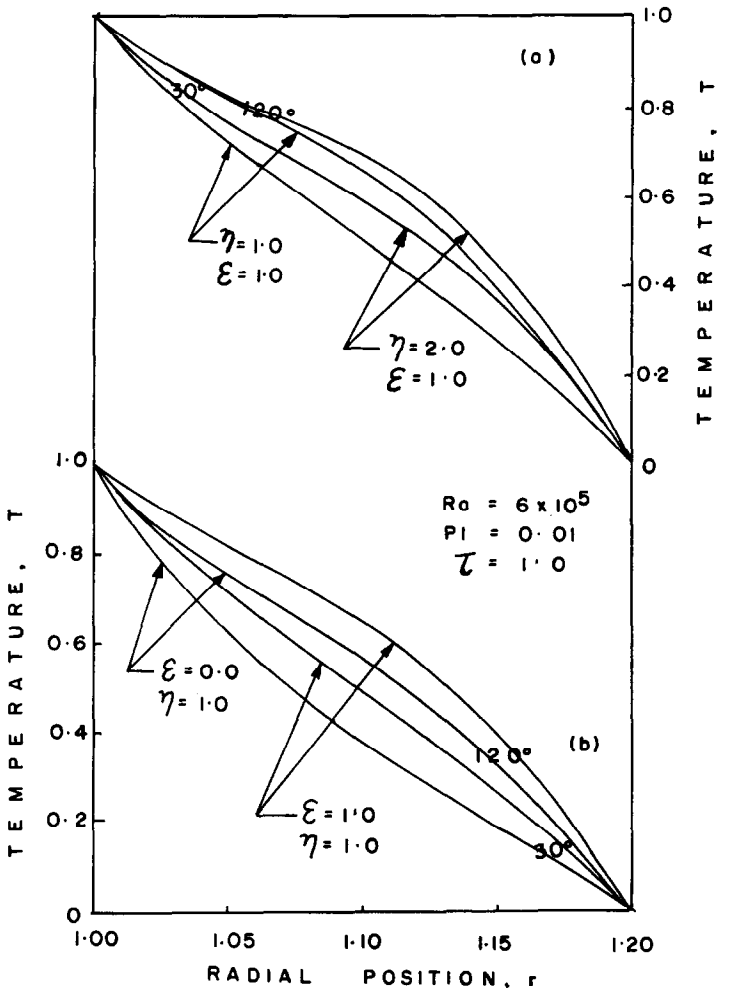

FIG. 8. Temperature profiles for angular positions of 30° and 120°. (a) Effect of degree of non-grayness of fluid; (b) effect of boundary surface emissivity.

higher value of Rayleigh number, 6×10^5, and the same radius ratio there was no evidence of the presence of secondary flow.

For the numerical tests carried out, the maximum value of the ratio of tangential radiative flux to radial radiative flux is 3.5% occurring at an angular position of 85° for the cases where $Pl = 0.01$. Since this percentage is small, the plots for q_θ/q_R are not presented, however, it is expected that the ratio will increase for higher values of R and Ra.

The temperature curves give a fair insight into the behaviour of the convective Nusselt number because this quantity, as defined, is proportional to the temperature gradient at the boundaries. Typical temperature plots are given in Figs. 7 and 8 representing temperature profiles for angular positions of 30° and 120°. Figure 7 shows the effects of the Planck number and optical thickness, while Fig. 8 shows the effects of the degree of nongrayness of the fluid and the boundary surface emissivity. Increasing radiation by decreasing Pl, increasing τ, or increasing η, will decrease the temperature gradient on the inner boundary while increasing the temperature gradient on the outer boundary. Decreasing boundary emissivity produces the opposite effect. These figures also indicate that radiation tends to smooth the temperature gradient of the bulk of the fluid hence reducing the effective buoyancy forces. This results in a decrease of the fluid motion which is due to buoyancy.

Acknowledgement—The author is grateful to the Director of the University of Nigeria's Computing Centre for the unlimited use of the computing facilities at the University of Nigeria.

REFERENCES

1. M. R. Abbot, A numerical method for solving the equations of natural convection in a narrow concentric cylindrical annulus with a horizontal axis, *Q. Jl Mech. appl. Math.* **17**, 471–481 (1964).
2. E. H. Bishop, C. T. Carley and R. E. Powe, Natural convection oscillatory flow in cylindrical annuli, *Int. J. Heat Mass Transfer* **11**, 1741–1752 (1968).

3. R. E. Powe, C. T. Carley and E. H. Bishop, Free convective flow patterns in cylindrical annuli, *J. Heat Transfer* **91,** 310–314 (1969).
4. R. E. Powe, C. T Carley and S. L. Carruth, A numerical solution for natural convection in cylindrical annuli, *J. Heat Transfer* **93,** 210–220 (1971).
5. J. R. Custer and E. J. Shaughnessy, Thermoconvective motion of low Prandtl number fluids within a horizontal cylindrical annulus, *J. Heat Transfer* **99,** 596–602 (1977).
6. I. C. Walton, The stability of free convection in a horizontal cylindrical annulus, *Q. Jl Mech. appl. Math.* **33,** 125–139 (1980).
7. C. H. Cho, K. S. Chang and K. H. Park, Numerical simulation of natural convection in concentric and eccentric horizontal cylindrical annuli, *J. Heat Transfer* **104,** 624–630 (1982).
8. M. A. Heaslet and R. F. Warming, Theoretical predictions of radiative transfer in a homogeneous cylindrical medium, *J. quant. Spectrosc. radiat. Transfer* **6,** 751–774 (1966).
9. I. S. Habib and R. Greif, Nongray radiative transport in cylindrical media, *J. Heat Transfer* **92,** 29–32 (1970).
10. A. T. Wassel, D. K. Edwards and I. Catton, Molecular gas radiation and laminar or turbulent heat diffusion in a cylinder with internal heat generation, *Int. J. Heat Mass Transfer* **18,** 1267–1276 (1975).
11. R. Echigo, S. Hasegawa and K. Kamiuto, Composite heat transfer in a pipe with thermal radiation of two-dimensional propagation—in connection with the temperature rise in flowing medium upstream from heating section, *Int. J. Heat Mass Transfer* **18,** 1149–1159 (1975).
12. M. Perlmutter and J. R. Howell, Radiative transfer through gray gas between concentric cylinders using Monte Carlo, *J. Heat Transfer* **86,** 169–179 (1964).
13. J. Higenyi and Y. Bayazitoglu, Differential approximation of radiative heat transfer in a gray medium, *J. Heat Transfer* **102,** 719–723 (1980).
14. M. M. Gibson and J. A. Monahan, A simple model of radiation heat transfer from a cloud of burning particles in a confined gas stream, *Int. J. Heat Mass Transfer* **14,** 141–147 (1971).
15. F. H. Azad and M. F. Modest, Evaluation of the radiative heat flux in absorbing, emitting and linearly-anisotropically scattering cylindrical media, *J. Heat Transfer* **103,** 350–356 (1981).
16. V. S. Arpaci and D. Gozum, Thermal stability of radiating fluids: the Bénard problem, *Phys. Fluids* **16,** 581–589 (1973).
17. S. Orzag and M. Israeli, Numerical simulation of viscous incompressible flows, *A. Rev. Fluid Mech.* **6,** 281–318 (1974).
18. G. de Vahl Davis, Laminar natural convection in an enclosed rectangular cavity, *Int. J. Heat Mass Transfer* **11,** 1675–1693 (1968).
19. C. Prakash and S. V. Patankar, Combined free and forced convection in vertical tubes with radial internal fins, *J. Heat Transfer* **103,** 566–572 (1981).
20. S. S. Kwon, T. H. Kuehn and T. S. Lee, Natural convection in the annulus between horizontal circular cylinders with three axial spacers, *J. Heat Transfer* **104,** 118–124 (1982).
21. S. O. Onyegegbu, Convective instability of rotating radiating fluids, *J. Heat Transfer* **102,** 268–272 (1980).

HMT 236

TRANSFERT THERMIQUE DANS UN ESPACE ANNULAIRE HORIZONTAL EN PRESENCE DE RAYONNEMENT THERMIQUE ET DE GRAVITE

Résumé—On étudie analytiquement le transfert thermique dans un fluide de Boussinesq non gris, absorbant et émettant à l'intérieur d'un espace annulaire entre deux cylindres concentriques, horizontaux, isothermes et infiniment longs. On emploie l'approximation de Milne–Eddington pour exprimer le transfert radiatif bidimensionnel en incluant le rayonnement radial et tengentiel. Les résultats montrent que la décroissance du nombre de Planck, l'accroissement du degré de non grisaille du fluide ou l'augmentation de l'épaisseur optique, accroît le transfert thermique total et réduit l'intensité de l'écoulement naturel induit et les vitesses. Une décroissance de l'émissivité des frontières produit l'effet inverse. Parce que le rayonnement décroît le nombre de Prandtl effectif d'un fluide, l'augmentation du rayonnement provoque un mouvement descendant du centre du tourbillon formé dans le case des fluides à nombre de Prandtl moyen comme l'air.

WÄRMEÜBERTRAGUNG IN EINEM HORIZONTALEN RINGRAUM DURCH NATÜRLICHE KONVEKTION UND STRAHLUNG

Zusammenfassung—Der Wärmeübergang im Ringraum zwischen zwei unendlich langen, horizontalen Zylindern mit einheitlicher Temperatur wird analytisch untersucht. Der Ringraum ist mit einem nichtgrauen (bezüglich Absorption und Emission) Boussinesq-Fluid gefüllt. Um die zweidimensionale Wärmeübertragung durch Strahlung, radial und tangential, auszudrücken, wird die Milne–Eddington-Näherung verwendet. Die Ergebnisse zeigen, daß mit abnehmender Planck-Zahl, zunehmender Transparenz des Fluids oder zunehmender optischer Schichtdicke der Wärmeübergang besser und die Intensität der Konvektionsströmungen geringer werden. Verringerte Emissivität der Oberflächen hat den gegenteiligen Effekt. Da die Strahlung die effektive Prandtl-Zahl des Fluids verringert, bewirkt eine Zunahme der Strahlung eine abwärts gerichtete Bewegung der Mitte von Wirbeln, wie sie bei Fluiden mit mittlerer Prandtl-Zahl, z. B. Luft, gebildet werden.

ТЕПЛОПЕРЕНОС ВНУТРИ ГОРИЗОНТАЛЬНОГО КОЛЬЦЕВОГО КАНАЛА С УЧЕТОМ ТЕПЛОВОГО ИЗЛУЧЕНИЯ И ПОДЪЕМНОЙ СИЛЫ

Аннотация—Аналитически изучается теплоперенос в поглощающей и излучающей несерой среде Буссинеска в кольцевом зазоре двух бесконечно длинных горизонтальных концентрических цилиндров. Для описания двумерного радиационного переноса с учетом радиальной и тангенциальной составляющих излучения применяется приближение Милна–Эддингтона. Результаты показывают, что уменьшение числа Прандтля, увеличение степени несерости среды или возрастание оптической толщины увеличивают суммарный теплоперенос и уменьшают интенсивность течения, вызванного подъемной силой, и скорость. Уменьшение излучательной способности границы дает обратный эффект. Поскольку излучение уменьшает эффективное число Прандтля жидкости, усиление излучения приводит к направленному вниз движению центра вихря, образованного в среде с числом Прандтля как у воздуха.